SAND2022-4226C

**Proceedings of the ASME 2022**
**Pressure Vessels & Piping Conference**
**PVP2022**
**July 17-22, 2022, Las Vegas, Nevada, USA**

**PVP2022-84635**

# DEVELOPMENT OF C-RING GEOMETRY TO EXPLORE FATIGUE CRACK EXTENSION AND VERIFICATION IN HIGH-PRESSURE VESSELS

**Robert W. Wheeler**
Hydrogen and Materials Science Department
Sandia National Laboratories
Livermore, CA 94550

**Joseph Ronevich**
Hydrogen and Materials Science Department
Sandia National Laboratories
Livermore, CA 94550

**Chris San Marchi**
Hydrogen and Materials Science Department
Sandia National Laboratories
Livermore, CA 94550

**Peter Grimmer**
Solid Mechanics Department
Albuquerque, NM 87123

**John M. Emery**
Materials and Failure Modeling Department
Albuquerque, NM 87123

## ABSTRACT

*High pressure hydrogen storage vessels are frequently retired upon reaching their designed number of pressure cycles, even in cases where the in-use pressure cycles are significantly less severe than the design pressure cycle. One method for extending the life of hydrogen vessels is recertification through non-destructive evaluation (NDE); however, NDE techniques are frequently evaluated with machined defects in test samples rather than fatigue cracks which occur during pressure cycling and may be more difficult to detect. In this paper, 50 mm wide ring sections (called C-rings, since they represent slightly more than half the circumference) were extracted from pressure vessels and mechanically cycled to establish fatigue cracks. Sub-millimeter starter notches were machined, via plunge electrical discharge machining (EDM), to control the location of crack initiation. Crack growth was monitored via direct current potential difference (DCPD) and backface strain gauges, both of which were shown to be good indicators for crack propagation. The C-ring geometry and fatigue crack growth were modeled to demonstrate the ability to monitor/control the crack length and area, which can be used to develop calibration samples of varying crack depth for NDE techniques. Additionally, this sample is intended to evaluate the influence of residual stresses on the sensitivity of NDE techniques, such as the design stresses in autofrettaged vessels.*

## NOMENCLATURE

| | |
|---|---|
| a | crack depth (through-wall) |
| DCPD | direct current potential difference |
| EDM | electro-discharge machining |
| NDE | non-destructive evaluation |

## 1. INTRODUCTION

High pressure hydrogen storage vessels, such as those used at hydrogen refueling stations, are retired upon reaching their designed number of pressure cycles, even in cases where the in-use pressure cycles are significantly less severe than the design pressure cycle [1-3]. One method for extending the life of hydrogen vessels is recertification through non-destructive evaluation (NDE) [4]. However, NDE techniques are frequently calibrated with samples containing machined defects rather than fatigue cracks [5-7]. While machining techniques such as plunge electro-discharge machining (EDM) and laser notching can provide repeatable sub-millimeter defects, there is a need for verification samples that contain sharp fatigue cracks with a known geometry. Additionally, a technique is needed to evaluate the ability of NDE methods to accurately detect fatigue cracks in the presence of compressive residual stresses induced by autofrettage processes or proof testing.

In this paper, a new "C-ring" sample geometry (Figure 1a) sectioned from a pressure vessel is proposed with the purpose of developing fatigue cracks in a controlled manner, such that a desired crack depth/area can be achieved. To this end, two C-ring samples were mechanically cycled to grow fatigue cracks of varying sizes, while the sample was monitored with direct current potential difference (DCPD) and backface strain gauges.




Sandia National Laboratories is a multimission laboratory managed and operated by National Technology & Engineering Solutions of Sandia, LLC, a wholly owned subsidiary of Honeywell International Inc., for the U.S. Department of Energy's National Nuclear Security Administration under contract DE-NA0003525.

The crack depths were controlled such that a calibration curve was established for both DCPD and the backface compliance.

The C-ring sample was developed and selected for three primary reasons. First, the geometry allows for relatively precise control over crack growth. While the DCPD was expected to be sufficient for monitoring crack growth, a backface strain gauge allowed for a direct comparison to crack growth simulations as well as provided a second predictive source for crack depth. Predicting (prior to destructive analysis) how far the crack has progressed through the sample would allow for grinding/polishing of the inner surface so that the machined flaw could be removed, leaving a fatigue crack of a desired depth. Second, the configuration can be prestressed to simulate autofrettage or statically loaded (either in tension or compression) during NDE. Lastly, this geometry allows for the validation of concurrent modelling efforts as it provides continuous fatigue crack growth data in a more representative sample (relative to conventional test specimens, such as a compact tension specimen).

To better understand the propagation of the crack in the C-ring sample, simulations were performed using Sierra/SM and FRANC3D [8,9]. Good qualitative agreement was observed between the simulated and experimental crack shape and quantitative agreement between the measured and predicted backface strain as a function of crack depth. Analysis of the stress intensity factors along the crack front as it moves through the thickness is also reported.

## 2. MATERIALS AND METHODS

A conventional, all-steel transportable pressure vessel (often referred to as a type 1 pressure vessel) with an outer diameter of 238 mm and wall thickness (t) of 14.5 mm was sectioned via electro-discharge machining (EDM) into 50.8 mm wide rings. Portions of the rings were then removed to give the samples a "C" shape, as shown in Figure 1a. Holes were added along the centerline of the ring to allow for mechanical loading via a ¾ in. bolt. After machining the C-ring geometry, a flaw or starter notch was manufactured by plunge EDM on the inside surface at the center of each C-ring specimen. Starter notches, shown in Figure 1b, were semi-elliptical with a 1.92 mm length (2c), 0.64 mm depth (a), and max root radius of 0.05 mm. This represents an initial flaw with aspect ratio of a/2c ~ 1/3.

To establish and grow a fatigue crack at the starter notch, the C-ring samples were mechanically cycled at peak loads ranging between 6.67 kN (1500 lbf) and 11.1 kN (2500 lbf) with a load ratio of R=0.1 (ratio of minimum to maximum applied load). DCPD and a backface strain gauge were implemented (as shown in Figure 2) to capture the initiation and growth of the fatigue crack. Both the strain gauge compliance and the relative DCPD change were monitored throughout fatigue cycling. Heat tinting (275°C / 30 min) was utilized to mark fatigue crack growth at specific stages of the test. At the conclusion of fatigue cycling, the C-ring samples were fractured open after immersion in $LN_2$.

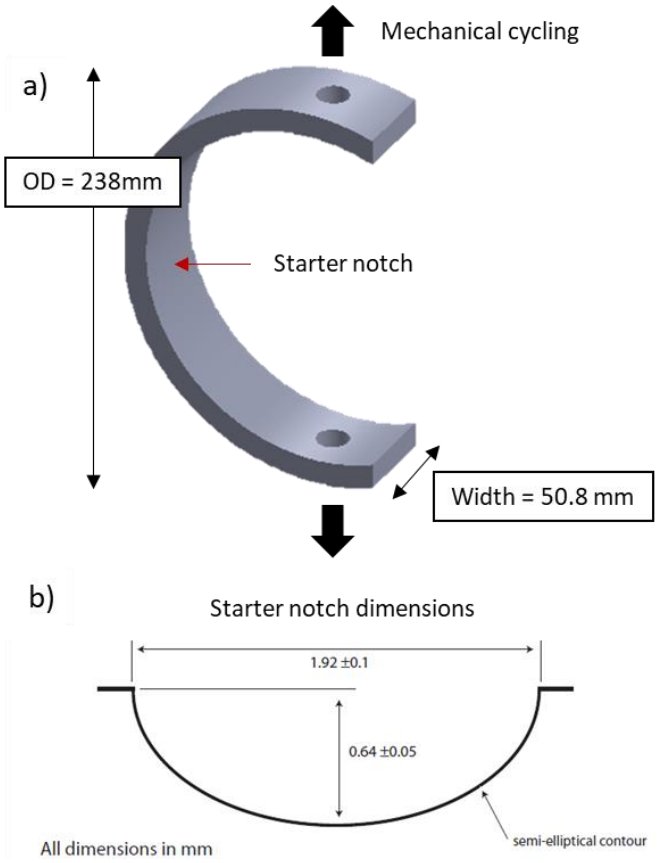


**FIGURE 1.** A) "C-RING" SAMPLE GEOMETRY. B) NOMINAL FLAW OR STARTER NOTCH DIMENSIONS.

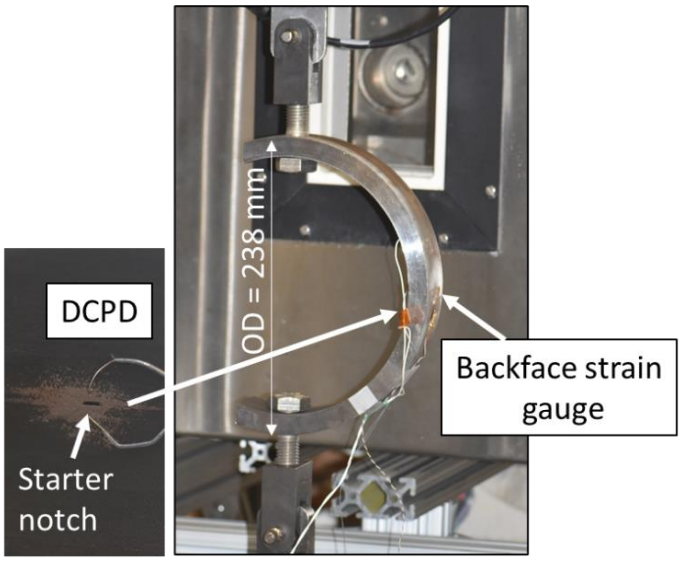


**FIGURE 2.** EXPERIMENTAL SETUP FOR C-RING SAMPLES, SHOWING DCPD AND BACKFACE STRAIN GAUGE LOCATION.

Finite-element analyses (FEA) of crack growth in the C-ring were conducted using Sierra/SM and FRANC3D. The

compressive strain measured by the backface strain gauge was compared to the simulated values and related to the crack depth. The experimental values were then compared to the FEA results.

## 3. RESULTS AND DISCUSSION

Two C-ring samples were mechanically cycled to induce fatigue cracks. Crack depth/area were varied in each sample and heat tinting was utilized to determine crack growth at various stages. Experimental results were supplemented with simulations that explored the crack growth morphology and sensitivity of the backface strain to crack depth.

### 3.1. Experimental Results

Mechanical cycling (R=0.1) at peak loads below 8.9 kN (2000 lbf) were found to have minimal impact on crack growth. As shown in Figure 3, the DCPD signal is largely unchanged for loads less than 8.9 kN. When the maximum load was increased to 8.9 kN (or higher), the DCPD signal increased monotonically, representing crack extension. The lack of crack extension at the lower loads is confirmed from compliance measurements: backface strain vs. applied load as shown in Figure 4. The compliance of the specimen (i.e., slope of the load-strain curve) is unchanged after cycling at the lower loads, indicating that a crack has not extended from the machined notch. After cycling at the highest load, however, the compliance has clearly changed, indicating significant crack extension from the machined notch.

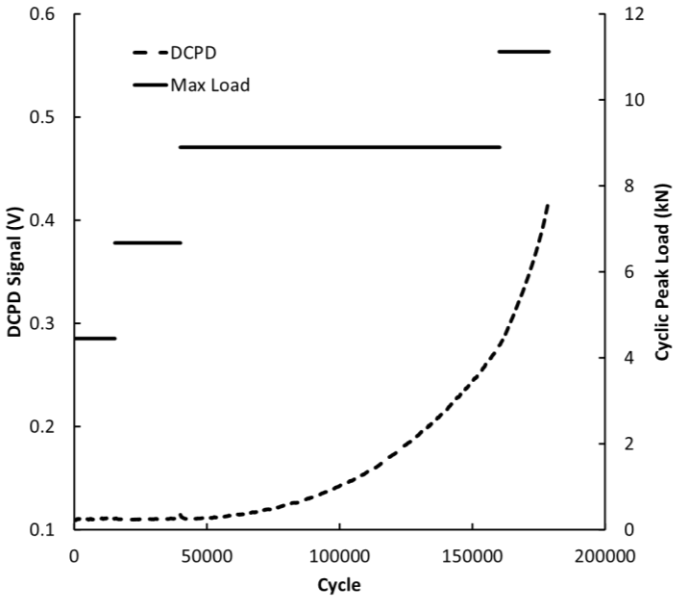


**FIGURE 3:** DCPD AND PEAK LOAD OVER THE COURSE OF FATIGUE CYCLING. SAMPLE 1.

After approximately 40,000 mechanical cycles with a peak load of 4.5 kN (1000 lbf) and 6.7 kN (1500 lbf), no change was detected in the backface strain or the DCPD. Once the peak load was increased to 8.9 kN (2,000 lbf), the DCDP gradually increased over approximately 120,000 cycles to more than double the initial value. Interestingly, the backface strain shows only a small (2-3%) increase in the compliance, as shown in the blue curve in Figure 4. After 18,000 cycles at 11.1 kN (2,500 lbf), the DCPD increased to more than 3.5 times its initial value. Similarly, the compliance, as measured by the backface strain gauge, nearly doubled after cycling at 11.1 kN (2,500 lbf). Additionally, the residual strain can be seen to increase from one cycle to the next in Figure 4, which shows approximately 10 mechanical cycles at each loading increment.

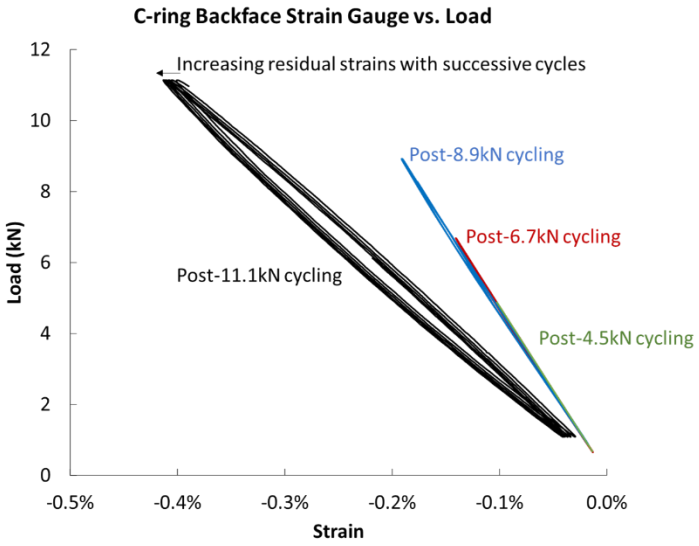


**FIGURE 4.** EXPERIMENTALLY MEASURED BACKFACE STRAIN VS. APPLIED LOAD AFTER FATIGUE CYCLING AT 4.5 kN (1000 LBF), 6.7kN (1500 LBF), 8.9kN (2000LBF), AND 11.1 kN (2500 LBF), AS SHOWN IN FIGURE 3. SAMPLE 1.

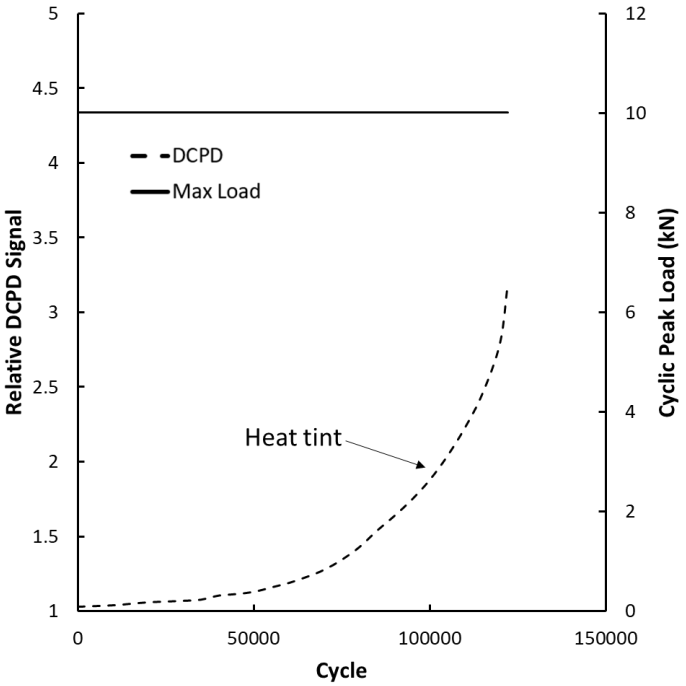


**FIGURE 5.** RELATIVE DCPD EVOLUTION FOR A C-RING CYCLED WITH A CONSTANT 10kN (2250 LBF) PEAK LOAD.

ARROW INDICATES WHEN SAMPLE WAS REMOVED FROM LOAD FRAME AND HEAT TINTED, WHICH CORRESPONDS TO THE DARKER REGION IN FIGURE 6B. SAMPLE 2.

The crack area was determined by breaking open the test specimen and determining the percentage of the cross-sectional area through which the crack had propagated. Following the 11.1 kN cycling on Sample 1, the crack area increased to over 30%, as shown in Figure 6a. A second sample was subjected to mechanical cycling with a maximum load of 10 kN (2,250 lbf) with a loading ratio of R=0.1 and interrupted for heat tinting partway through the cycling history. Therefore, two points in the crack extension history could be correlated with the strain and DCPD measurements. The evolution of the relative DCPD signal is shown in Figure 5, whereas the fracture surface is shown in Figure 6b, showing (i) the starter notch, (ii) a heat tinted area with a normalized crack area of about 11% and corresponding to a normalized DCPD of ~2 (as shown in Figure 7), and (iii) a final crack area of approximately 45% corresponding to a normalized DCPD signal of ~3.6.

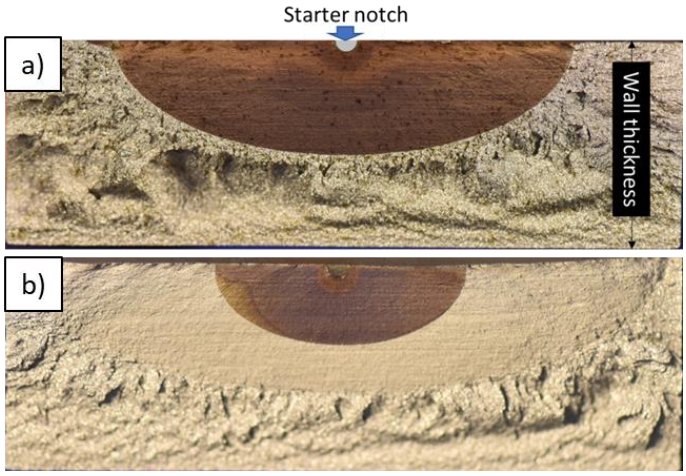


**FIGURE 6.** FRACTURE SURFACES OF C-RING A) SAMPLE 1 AND B) SAMPLE 2. HEATING TINTING WAS UTILIZED TO COLOR THE SURFACE FOR POST-MORTEM MEASUREMENTS. SAMPLES WERE FRACTURED OPEN WITH $LN_2$. CRACK AREA WAS CALCULATED USING NI VISION ASSISTANT.

Based on the heat tinted and final crack areas and the corresponding DCPD values, a linear calibration curve was assumed to relate the normalized DCPD values to the normalized crack area. This relationship is shown in Figure 7, which plots the DCPD vs. area for both samples and shows a relatively linear trend.

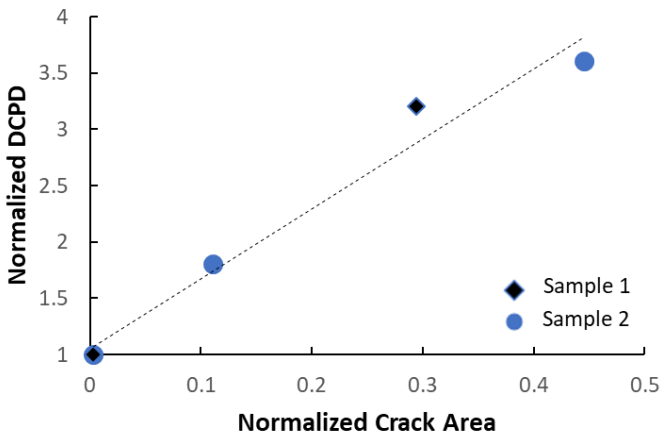


**FIGURE 7.** NORMALIZED DCPD (FINAL/ORIGINAL) VS. NORMALIZED CRACK AREA (FINAL/TOTAL) FOR BOTH C-RING SAMPLES. THE DCPD VALUES WERE NORMALIZED RELATIVE TO THE ORIGINAL VALUES FOR EACH TEST. THE DASHED LINE SHOWS AN APPROXIMATE LINEAR FIT TO THE DATA FROM BOTH SAMPLES.

### 3.2. Modeling Results and Comparison

The predicted crack shape is shown in Figure 8, including the nominal starter notch geometry. At first, the crack front at the deepest point of the crack grows fastest, but, as the crack evolves, the length dimension (2c) grows faster than the depth (a) due to the bending nature of the applied mechanical load. This results in the elliptical crack lengthening as it propagates towards the back surface, which can be qualitatively seen in Figure 6. Therefore, at early growth stages the crack shape maintains the aspect ratio of a/c ~ 1/3 but quickly evolves to a value a/2c < 1/3.

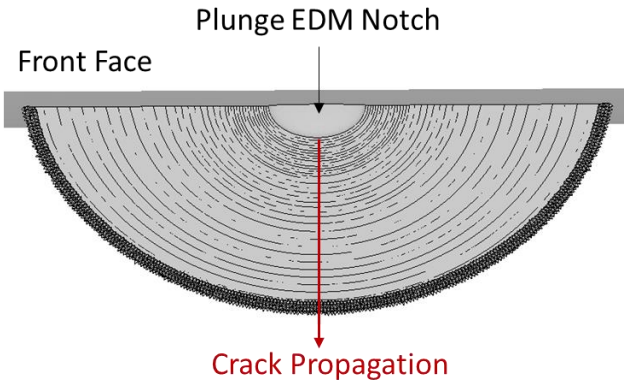


**FIGURE 8.** FE PREDICTED CRACK GROWTH (LOOKING DOWN ON THE CRACK PLANE).

While the DCPD was found to be relatively linear with crack area, the experimentally measured backface strain was significantly less sensitive during the initial crack growth. To better capture this response, the compressive backface strain was calculated for a 6.7kN load at crack growth increments of approximately a/t = 0.01 from the starter notch up to about a/t =

0.6. The resulting predicted backface strain is shown in Figure 9 (dashed line) along with the experimentally measured strains (blue symbols).

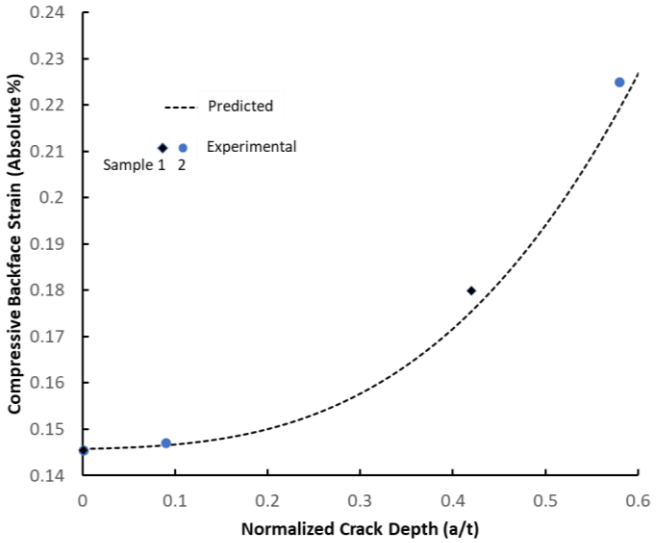


**FIGURE 9**. COMPRESSIVE BACKFACE STRAIN AT 6.7KN (1502LBF) VS. NORMALIZED CRACK DEPTH (DEPTH/WALL THICKNESS).

As expected, both the predicted and experimental strains are increasingly sensitive to crack growth as the crack extends. While there are very noticeable changes in the strains as the crack extends beyond about a/t = 0.2, the relatively small changes in backface strain for crack lengths below 20% make it difficult to detect initiation and to monitor crack growth. In contrast, the DCPD signal appears to evolve almost linearly from the onset of crack growth.

As shown Figures 6 and 8, the cracks initially have a semi-circular profile and, as the crack propagates through the thickness, the profile becomes more elliptical and grows more quickly towards the edges (i.e., in the length dimension). The evolution of the mode I stress intensity factor can be seen in Figure 10 for increasing crack depth (a/t) with a constant load (6.7 kN). Initially, the stress intensity factor is highest at the center of the crack; however, as the crack propagates deeper into the sample, the stress intensity factor becomes higher on the edges. The bending nature of the applied mechanical load induces compressive stresses at the backface, which contains growth in the depth direction, resulting in higher $K_I$ at the edges and faster crack growth in the crack length direction.

### 3.3. Potential Uses of C-ring Geometry

The C-ring geometry and this combined crack monitoring approach shows promise for the development of NDE

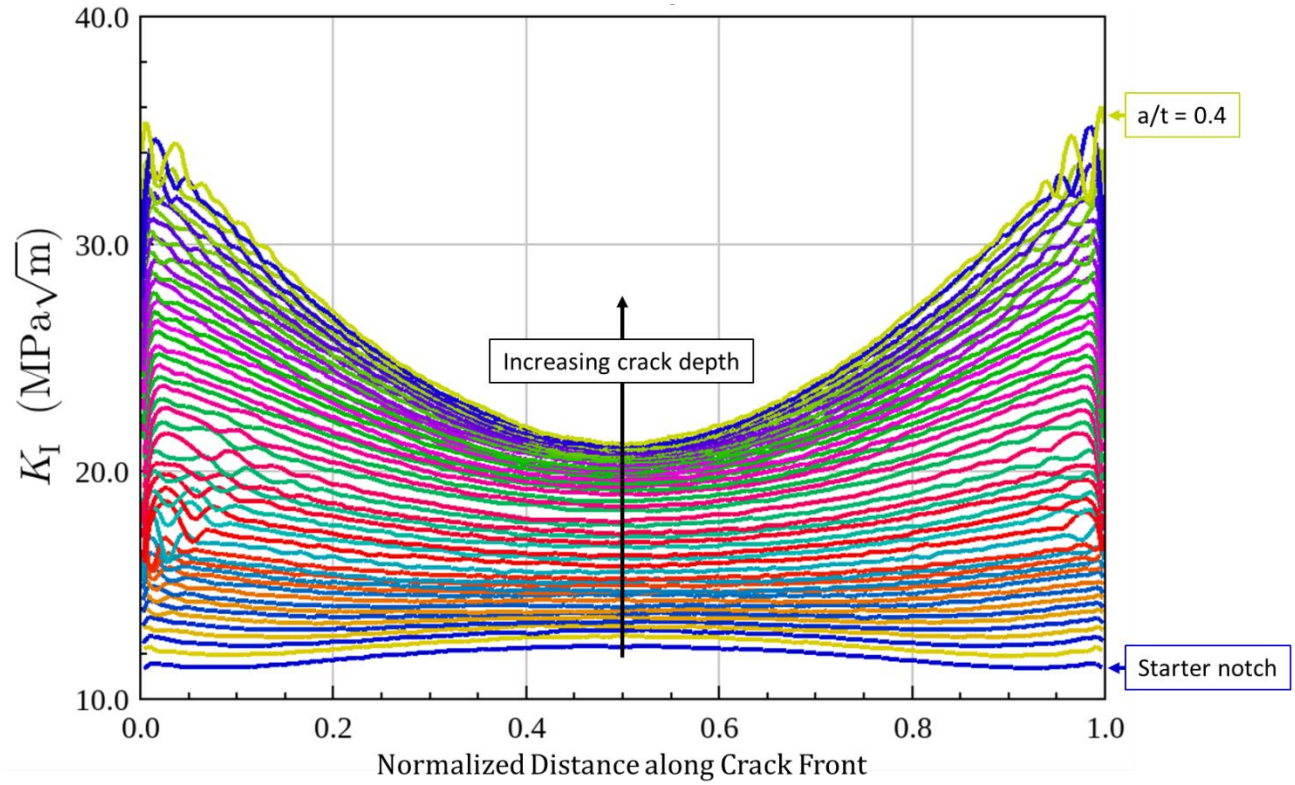


**FIGURE 10.** MODE I INTENSITY FACTOR FOR AN APPLIED LOAD OF 6.7 kN (1502LBF) FOR CRACK DEPTHS RANGING FROM THE STARTER NOTCH (A/T = 0.044) TO 40% THROUGH THICKNESS, PLOTTED ON THE NORMALIZED DISTANCE ALONG THE CRACK FRONT. 0.5 REPRESENTS THE CENTER (DEEPEST) PART OF THE CRACK FRONT WHILE 0.0 AND 1.0 REPRESENT THE EDGES ON THE FRONT FACE.

verification specimens with known fatigue cracks instead of machined defects. The DCPD had greater sensitivity to early crack growth and displayed a linear relationship with crack area. The backface strain gauge showed less sensitivity at smaller crack areas, but the sensitivity improved for crack depth greater than about a/t = 0.2. While the depths of the starter notches were approximately 5% of the thickness, fatigue cracks were grown to depths of between 10 and 60%. Both the relative DCPD and backface compliance showed clear trends that can be used to estimate the crack area and depth, respectively.

Using this C-ring geometry, one could extend cracks to prescribed flaw depths using fatigue cycling, which could then be inspected via NDE methods (e.g., eddy current). The machined notch could be removed via grinding or polishing so that only the fatigue crack remains. In addition, the unique nature of the C-ring allows for either static compressive or tensile loading such that flaws could be scanned concurrent with applied stresses that represent residual stresses. For example, a threaded rod could be used to place the inner surface in compression to represent the residual stress resulting from proof testing or autofrettage. This configuration would enable evaluation of the NDE technique in different pre-stressed conditions. At the completion of NDE, the C-ring can be heat tinted and fractured open to calibrate the measurements from NDE to the true crack size. Future research for this effort includes evaluation of NDE methods (e.g., eddy current) and integration with fatigue crack growth modeling.

## 4. CONCLUSION

In this paper, a C-ring specimen was extracted from an all steel (type 1) pressure vessel and mechanically cycled to induce fatigue crack growth. Throughout the test, the DCPD and backface strains were monitored to study their evolution. With post-mortem analysis, these techniques were characterized with respect to physical measurements of crack area and crack depth. A linear trend was observed between the DCPD and crack area suggesting DCPD is a sensitive method to characterize crack initiation and growth (especially in early stages of growth). In contrast, the backface strain was not sensitive to the early stages of crack growth. Finite-element analyses of crack growth in the C-ring sample were performed to relate the backface strain to the crack depth, and good agreement was shown between the experimental results and simulations. Analysis of the stress intensity factors on the crack front indicates that, as the crack front propagates, it lengthens at an increasing rate. This trend is also evident in post-mortem observation of the crack shape. This combined approach of DCPD and backface compliance provides a more versatile means of evaluating the sensitivity of NDE techniques to real fatigue cracks. Additionally, the method provides an opportunity to pre-stress the crack concurrently with NDE inspection.


## ACKNOWLEDGEMENTS

Sandia National Laboratories is a multimission laboratory managed and operated by National Technology and Engineering Solutions of Sandia, LLC., a wholly owned subsidiary of Honeywell International, Inc., for the U.S. Department of Energy's National Nuclear Security Administration under contract DE-NA-0003525. This work is supported by the U.S. Department of Energy, through the Office of Energy Efficiency and Renewable Energy's (EERE) Hydrogen and Fuel Cell Technologies Office (HFTO). This paper describes objective technical results and analysis. Any subjective views or opinions that might be expressed in the paper do not necessarily represent the views of the U.S. Department of Energy or the United States Government.


## REFERENCES


[1] Boiler and Pressure Vessel Code, Section VIII - Rules for Construction of Pressure Vessels, Division 3 - Alternative Rules for Construction of High Pressure Vessels, ASME, 2019.

[2] San Marchi, C., Ronevich, J., Bortot, P., Wada, Y., Felbaum, J., and Rana, M., "Technical basis for master curve for fatigue crack growth of ferritic steels in high-pressure gaseous hydrogen in ASME section viii-3 code" (PVP2019-93907). ASME Pressure Vessels and Piping Conference, San Antonio TX, 17-24 July 2019.

[3] Ronevich, J. A., San Marchi, C., Brooks, D., Emery, J. M., Grimmer, P., Chant, E., Sims, J. R., Belokobylka, A., Farese, D., and Felbaum, J., "Exploring life extension opportunities of high-pressure hydrogen pressure vessels at refueling stations" (PVP2021-61815). ASME Pressure Vessels and Piping Conference, virtual, 13-15 July 2021.

[4] ASME PCC-3-2017 Inspection Planning Using Risk-Based Methods, ASME, 2017.

[5] Sophian, A., Tian, G., & Fan, M. (2017). Pulsed eddy current non-destructive testing and evaluation: A review. Chinese Journal of Mechanical Engineering, 30(3), 500-514.

[6] Yuan, F., Yu, Y., Li, L., & Tian, G. (2021). Investigation of DC electromagnetic-based motion induced eddy current on NDT for crack detection. IEEE Sensors Journal, 21(6), 7449-7457.

[7] Xu, Y., Yang, Y., & Wu, Y. (2020). Eddy Current Testing of Metal Cracks Using Spin Hall Magnetoresistance Sensor and Machine Learning. IEEE Sensors Journal, 20(18), 10502-10510.

[8] 2009. ABAQUS/Standard User's Manual. Dassault Systémes Simulia Corp, United States.

[9] Fracture Analysis Consultants, I. FRANC3D.